Chapter 3

Dual-Core Transversally Chirped Microstructured Optical Fiber for Mode-Converter Device and Sensing Application

Erick Reyes Vera, Juan Úsuga Restrepo, Margarita Varon and Pedro Torres

Additional information is available at the end of the chapter

http://dx.doi.org/10.5772/intechopen.70989

Abstract

We propose and demonstrate the concept of transversally chirped microstructured optical fiber and its application for the development of new platforms for sensing and telecommunications devices. First, the feasibility of the structure is demonstrated through two different techniques of manufacture. Based on the proposed structure, a novel mode-converter device is numerically studied. It is found that the mode conversion between LP_{01} and LP_{11} modes can be continuously tuned by temperature changes from 25 to 75°C. And that, the coupling efficiency in the wavelength range between 1.2 μm and 1.7 μm is always higher than 65%. Consequently, the proposed mode converter can operate in the E + S + C + L + U bands. Finally, a similar structure was used to design a new sensing architecture, which consisting of a dual-core transversally chirped microstructured optical fiber for refractive index sensing of fluids. We show that by introducing a chirp in the hole size, the microstructured optical fiber can be a structure with decoupled cores, forming a Mach–Zehnder interferometer in which the analyte directly modulates the device transmittance by its differential influence on the effective refractive index of each core mode. We show that by filling all fiber holes with analyte, the sensing structure achieves high sensitivity (transmittance changes of 302.8 per RIU at 1.42) and has the potential for use over a wide range of analyte refractive index.

Keywords: microstructured optical fibers, fiber optics sensors, interferometry, mode converter, space, division multiplexing, refractive index sensor, mode conversion, Mach–Zehnder interferometer

1. Introduction

In the last two decades, several technological breakthroughs were needed to increase and satisfy the capacities of the optical links. Some important advances allow the connection between users through the implementation of optical fibers. One of the most important advances, related to these technological breakthroughs, is the use of broadband optical amplifiers to increase the length of optical links. On the other hand, different multiplexing techniques such as optical time division multiplexing (OTDM), wavelength division multiplexing (WDM) and polarization division multiplexing (PDM) have been implemented in transmission channels to increase the optical transmission system capacity. However, due the high growth in the demand, the transmission capacity of this technology has reached the limits imposed by the nonlinear effects in optical fiber [1, 2]. In order to keep up the growth of current optical communication networks, it is necessary to implement new technological breakthroughs. One possibility is the implementation of independent spatial channels to send information. This technique is known as spatial division multiplexing (SDM) and can be implemented in two different schemes. Intuitively, in the multi-core fiber (MCF) scheme, each core acts as an independent channel for sending the information [1], while in the modal division multiplexing (MDM) scheme, each mode is considered an independent transmission channel as in single-mode fiber [3, 4]; hence, the key is to convert the fundamental fiber modes to higher order modes. As the processing systems are not prepared to work with hundreds of modes, in the MDM scheme it is preferred to work with few modes fibers (FMFs) [3, 4]. As with any new technology, emerging SDM systems require the development of new components such as optical fibers that support multiple spatial modes and integrated mode converters to control propagating modes, spatial mode multiplexers (SMUXs) and demultiplexers (SDEMUXs).

To address these needs, several works have reported different mechanisms to control the propagation modes in FMFs, such as long period fiber grating (LPFG), Fiber Bragg Gratings (FBG), tapers and phase mask [5–10]. Another interesting alternative is to use microstructured optical fibers (MOFs), also called photonic crystal fibers (PCFs), which offer flexibility in its design and the possibility of manipulating the optical properties of the device because its characteristics—dispersion, effective area, birefringence and nonlinearity, among others—depends on the diameter of holes, the separation between them and the shape of the microstructure [11–17]. Owing these characteristics, these type of optical fibers have been employed for the development of different devices such as polarization beam splitters [18], dispersion compensators [19, 20] and mode converters [5] to name a few.

Mode selective couplers (MSC) based on microstructured optical fiber (MOF) represent one of the best approaches to achieve mode conversion, avoiding the problems of other techniques—bulky free-space optics, polished- and fused-type MSC—since the devices are compact, robust and efficient, and allows the possibility of manipulating its behavior based on the MOF geometrical parameters [3, 21–24]. The principle of MSC is to phase match the fundamental mode in a single-mode fiber with a high-order mode in FMF.

In [23], Cai et al. proposed a mode converter based on a hybrid dual-core MOF, which contains an index-guided core and a photonic bandgap core. The air holes of the first ring

around one of the cores are replaced with high-index rods, then mode conversions can be continuously achieved by varying the refractive index of high-index rods The all-solid bandgap structure requires two suitable materials that are also compatible for drawing and splicing with few-mode fibers. In [24], the authors proposed a tuneable MSC based on a fully liquid-filled dual-core MOF with non-identical cores. The tuning of the wavelength in the S + C + L + U bands is performed by changing the refractive index (RI) of the filling fluid.

Simultaneously, the implementation of MOFs has allowed the development of a new family of optical fiber sensors, which present higher sensitivity and compact sizes compared to sensors based in standard optical fibers and other technologies [25]. Some novel configurations of these sensors have been implemented in the measurement of refractive index (RI) changes [26, 27], temperature [28, 29] and force [30–32], among others. The refractive index sensors are the most studied and applied in recent years in biological, medical and chemical applications [33–38]. Two general configurations for the interaction between the light and analyte in MOFs may be identified. In the first option, the analyte is located in the evanescent field of the waveguide [39, 40]. In the second option, the analyte can be inserted into the fiber holes and experience long range interaction with the guided light while maintaining the waveguide, thereby ensuring a robust device [26, 41]. In addition, optical fiber sensors based on the dual-core MOF configuration are able to achieve improved sensitivity for RI measurements. In these structures, the fiber holes are filled with the analyte. Then, the refractive index of the sample modulates the device transmittance by its influence on the coupling between the cores. In [37], Markos et al. presented an experimentally feasible design of a dual-core microstructured polymer optical fiber (mPOF), which can act as a label-free selective biosensor. Numerical results indicate a sensitivity of 20.3 nm/nm—wavelength shift per nm thickness of biolayer—achieved with a 15-cm-long device at visible region where the mPOF has the lowest absorbance. Recently, Wu et al. proposed and demonstrated a novel configuration with a sensitivity of 30,100 nm per refractive index unit (nm/RIU). This configuration is based on a directional coupler architecture using a solid- core PCF [42]. Yuan et al. demonstrated the design of an all-solid dual-core photonic bandgap fiber, in which a single hole between the cores acts as microfluidic channel for the analyte [43]. The predicted sensitivity was 70,000 nm/RIU. In 2011 [44], Sun et al. proposed and demonstrated a refractive index sensor based on the selectively resonant coupling between a conventional solid core and a microstructured core. Numerical results shown that this configuration could achieve a sensitivity of 8500 nm/RIU. However, these configurations have also some drawbacks, for instance, have complex design for the fiber cores or require selective filling. For this reason, the implementation of interferometric schemes in combination with these specialty fibers has emerged as a new alternative. In [26], we introduced the concept of transversally chirped solid-core MOF and reported a dual-core chirped MOF that could act as a structure with decoupled cores, thus forming a Mach-Zehnder interferometer in which the analyte directly modulated the device transmittance by its differential influence on the effective RI of each core mode, achieving a sensitivity of 300 per RIU for a 12-mm-long device and analyte RI of 1.42. A year later, we designed a label-free biosensor by immobilization of an antigen sensor layer onto the walls of the air holes of rings surrounding one core of the fiber. A sensitivity of around 3.7 nm/nm was achieved for a 10 mm

long device at near IR wavelengths [38]. Then, we studied some refractometric properties of these configuration using numerical models to improve the performance of this device [41].

The chirp concept has been widely used in one-dimensional structures such as chirped mirrors [45] and chirped fiber Bragg gratings where different spectral components are localized at different positions inside the chirped structure [46]. In both cases, the chirp was implemented on the propagation direction. Chirping also has already been applied for designing hollow core fibers with a radially chirped microstructured cladding [47]. By introducing a radial chirp into the photonic crystal structure, it was demonstrated a novel concept that breaks with the paradigm of lattice homogeneity and enables a new degree of freedom in the design of MOFs. Another important variation was reported by Ghosh et al. [48]. The authors proposed a novel chirped cladding as a novel tailoring tool to attain wider transmission window and reduced temporal dispersion in an all-solid Bragg-like MOF.

In this chapter, dual-core transversally chirped MOFs for active mode conversion in telecommunications and sensing applications are presented. In the first part of this chapter, we explain the fabrication process of this novel structure. Next, we demonstrate that this type of MOF can be used to design a novel and tuneable mode-converter to improve the performance of the modern optical systems. Finally, a dual-core transversally chirped MOF is proposed to create a compact highly sensitivity optical fiber sensor.

2. Fabrication methodology

Two techniques can be used to fabricate dual-core transversally chirped MOFs. The first alternative consists in the implementation of the standard stack and draw technique [49, 50]. The first step is producing the preform, which is based on stacking of capillaries and rods. In our case, the diameter of the capillary should have a slight reduction in its diameter along the cross-section. Then, several slightly chirped preforms of about 1 mm were obtained by pulling a ~1 cm preform with a small transversal temperature gradient. The temperature gradient was produced by pulling the preform off-center [26]. After this process the fiber shown in **Figure 1(a)** was obtained, which is characterized by a slight transverse chirp in the hole distribution.

The second alternative consists in tapering the MOF from the previous step, in such a way that fiber structures with a larger transverse chirp can be achieved. In our case, MOF tapers were produced by using the flame brushing technique. The MOF was mounted on a motorized stage. The fiber was heated using a butane flame, which was mounted on a second motorized stage. The butane flame was moved back and forth along the fiber axis as the taper was pulled simultaneously. In order to ensure that the holes do not collapse, it was applied pressure within the holes. **Figures 1(b)** and **(c)** show the cross-section of two tapered MOFs obtained with an applied pressure of 6 and 7 bars, respectively. From these results, it is evident that the pressure applied inside of fiber holes can control the transversal chirp of the pristine MOF. For example, the MOF with an applied pressure of 6 bars has a structure in which none

http://dx.doi.org/10.5772/intechopen.70989

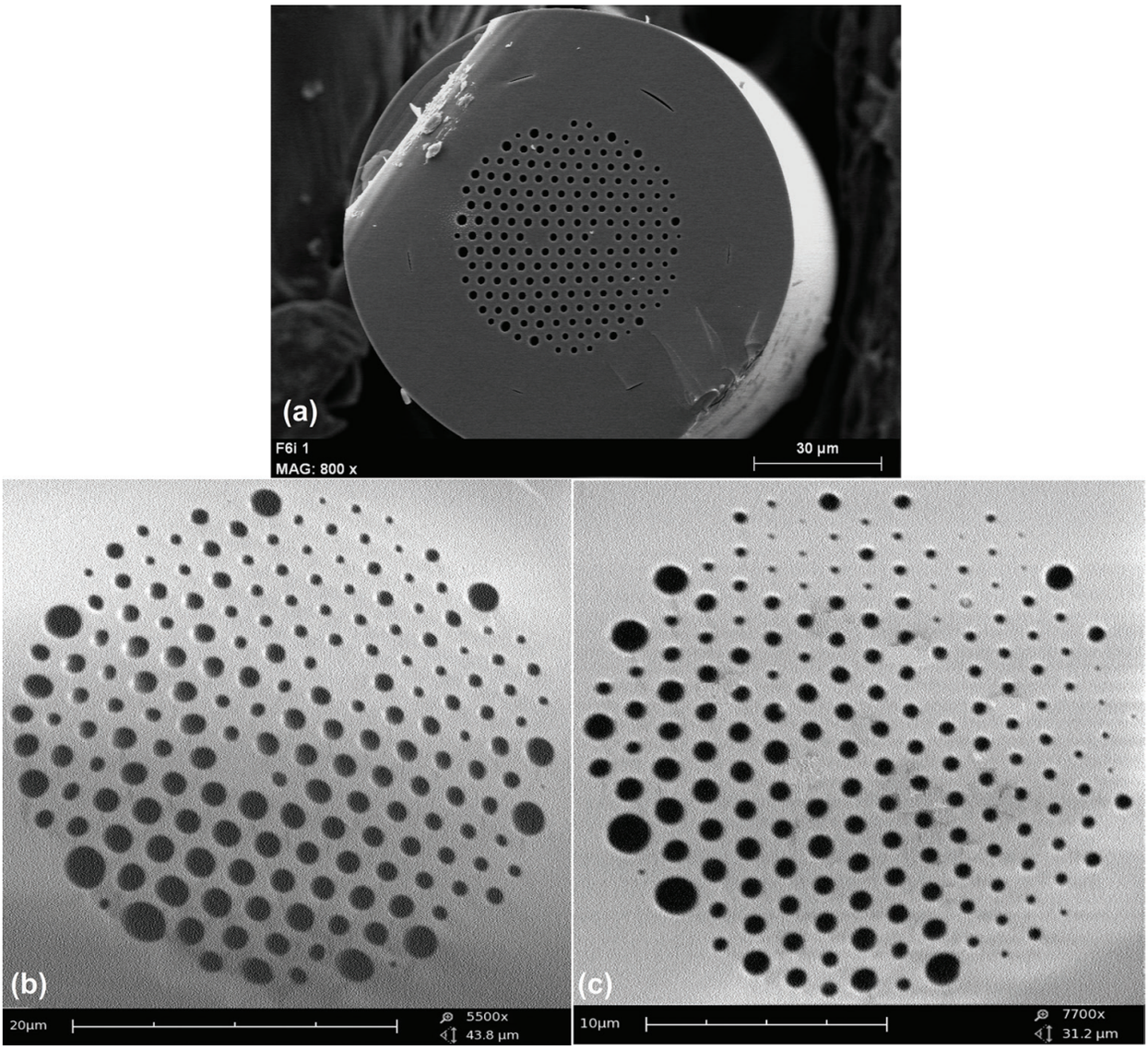

Figure 1. SEM images of (a) a dual-core transversally chirped MOF obtained with the standard stack and draw technique. (b) and (c) Dual-core transversally chirped MOF tapers obtained through the flame brushing technique at 6 and 7 bars, respectively, within the fiber holes.

of the holes collapsed during the tapering process and the transverse chirping slope is smaller than the MOF obtained when the pressure was 7 bars.

3. Mode converter device

The cross-section of the proposed dual-core transversally chirped MOF MSC is shown in **Figure 2**. As we can see, the cladding holes are arranged in a hexagonal lattice with constant pitch Λ = 6 μm. The diameter of the circular air holes decreases linearly from d_{max} = 6 μm on the left side of the fiber to d_{min} = 0.9 μm on the right side. The considered MOF has two solid

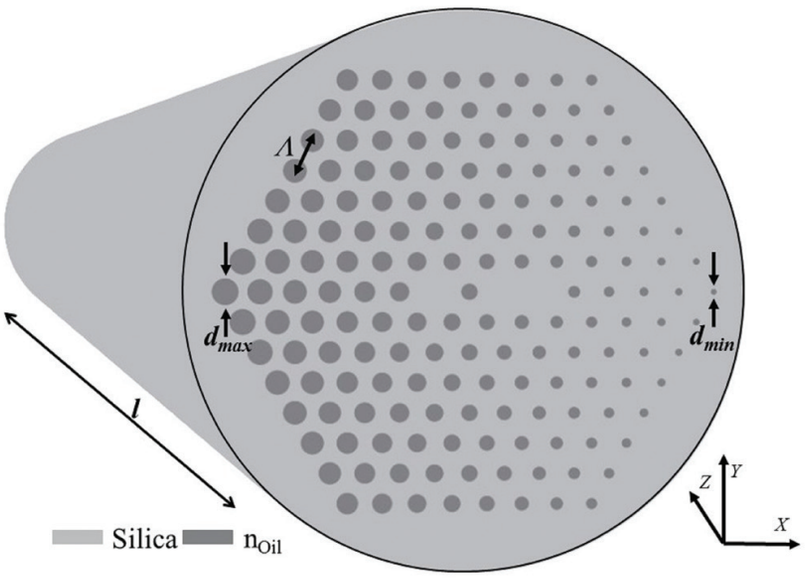

Figure 2. Structure of the mode selective coupler based on a dual-core transversally chirped MOF.

cores, which are separated by only one hole in the microstructure, that is, by 2Λ. In this case, we employ a small separation between both cores in order to guarantee power transfer. In addition, background material is silica, and its dispersion is given by Sellmeier's equation [51]. Note that by the transverse chirping of the microstructure, the fiber cores obviously do not have the same shape. In this case, the right core is almost 1.8 times wider than the left core.

In our device, a RI-matching oil (Cargille Labs., $n_0 = 1.42$ at room temperature) is chosen to be filled onto the MOF, and its thermo-optic coefficient is $\alpha = 3.94 \times 10^{-4}$/C°, and the relationship between refractive index n and temperature T is to be $n = n_0 - \alpha(T - T_0)$ where T_0 is the room temperature. A variety of functional fiber devices have been fabricated based on MOF fully infiltrated by fluid such as optical switches [52, 53], all-optical modulator [54], tunable optical filters [55] and fiber polarimeters [56].

According to our design, the fundamental mode LP_{01} in the left core is converted to the LP_{11} mode in the right core. Because the right core supports two modes (LP_{01} and LP_{11}), supermode analysis [57] was used to investigate the behavior of the temperature-controlled mode converter. We performed finite element simulations under different temperature conditions at the particular free-space wavelength $\lambda = 1.55$ μm.

Figure 3 shows the effective index curves of symmetric (supermode 1) and antisymmetric (supermode 2) modes. From these results, it is evident that LP_{01} mode in the left core interacts with LP_{11} mode in the right core. As expected, the effective refractive index n_{eff} of both supermodes decrease with increasing temperature. In addition, the effective index of symmetric mode is always slightly larger than that of antisymmetric mode, indicating that these supermodes have different propagation constants and therefore there is a beating between these two modes and, thus, the power fluctuates back and forth between the two cores.

Once it was determined which modes exchange energy, the coupled mode theory was applied to find the phase-matching conditions [57, 58]. Here, each core is analyzed as an independent

http://dx.doi.org/10.5772/intechopen.70989

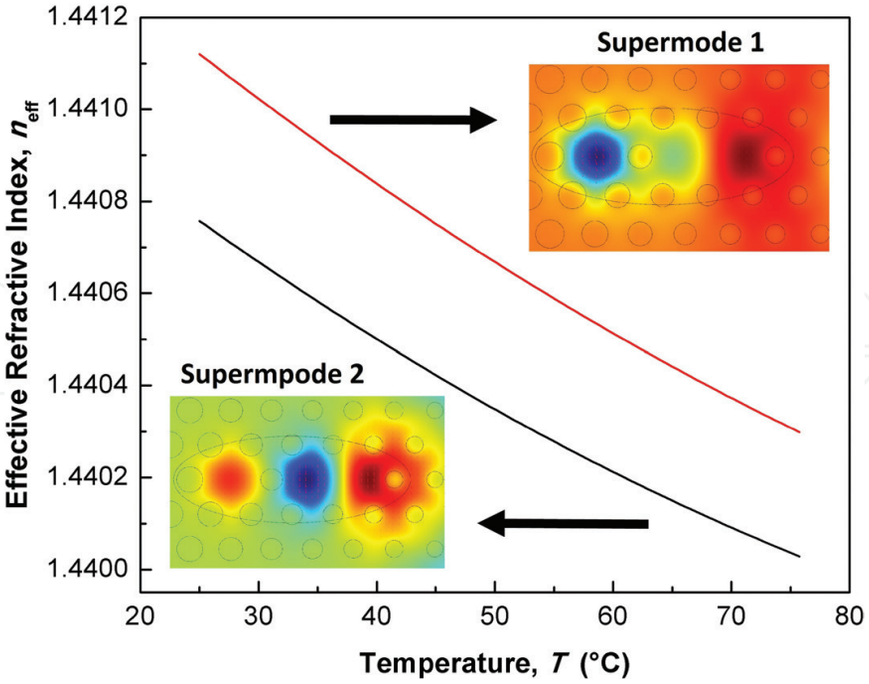

Figure 3. Supermode analysis of the dual core transversally chirped MOF when temperature varies from 25 to 75°C at an operating wavelength λ=1.55 μm.

waveguide to avoid the perturbations caused by the presence of the other core. When the mode of the left core interacts with the mode of the right core, crossing occurs and propagation constants of the two modes are matched. Then, maximum power transfer can be achieved at the phase-matching wavelength.

Figure 4(a) presents the modal dispersion curves of LP_{01} mode in the left core and of LP_{11} mode in the right core with different temperature values in the wavelength range 1.2–1.8 μm. Colored points in this figure represent the phase-matching wavelengths. **Figure 4(b)** shows the dependence of the operating wavelength on temperature. Therefore, the liquid-filling method is an easy method to tune the behavior of this device. According to this result, this mode converter could operate in the E + S + C + L + U bands.

To test the mode-conversion performance of the coupler, **Figure 5** presents the normalized power as a function of fiber length at a wavelength of 1.55 μm. It is observed that almost 100% of the power is coupled between the cores with the beating length L_c = 2 mm. This result shows that the proposed device is compact compared with other MOF-based mode converters [5, 7, 23–25].

Finally, the mode coupling efficiency of the device was evaluated. The results are depicted in **Figure 6**. From these results, it is evident that the mode coupling efficiency obtained with this structure presents a good performance in the E + S + C + L + U bands. As expected, the behavior of this device can be thermally controlled. It is observed that the phase-matching wavelength varies with the temperature change. It is found that when T increases, the operating wavelength also increases. In addition, coupling efficiencies above 65% were obtained in this study.

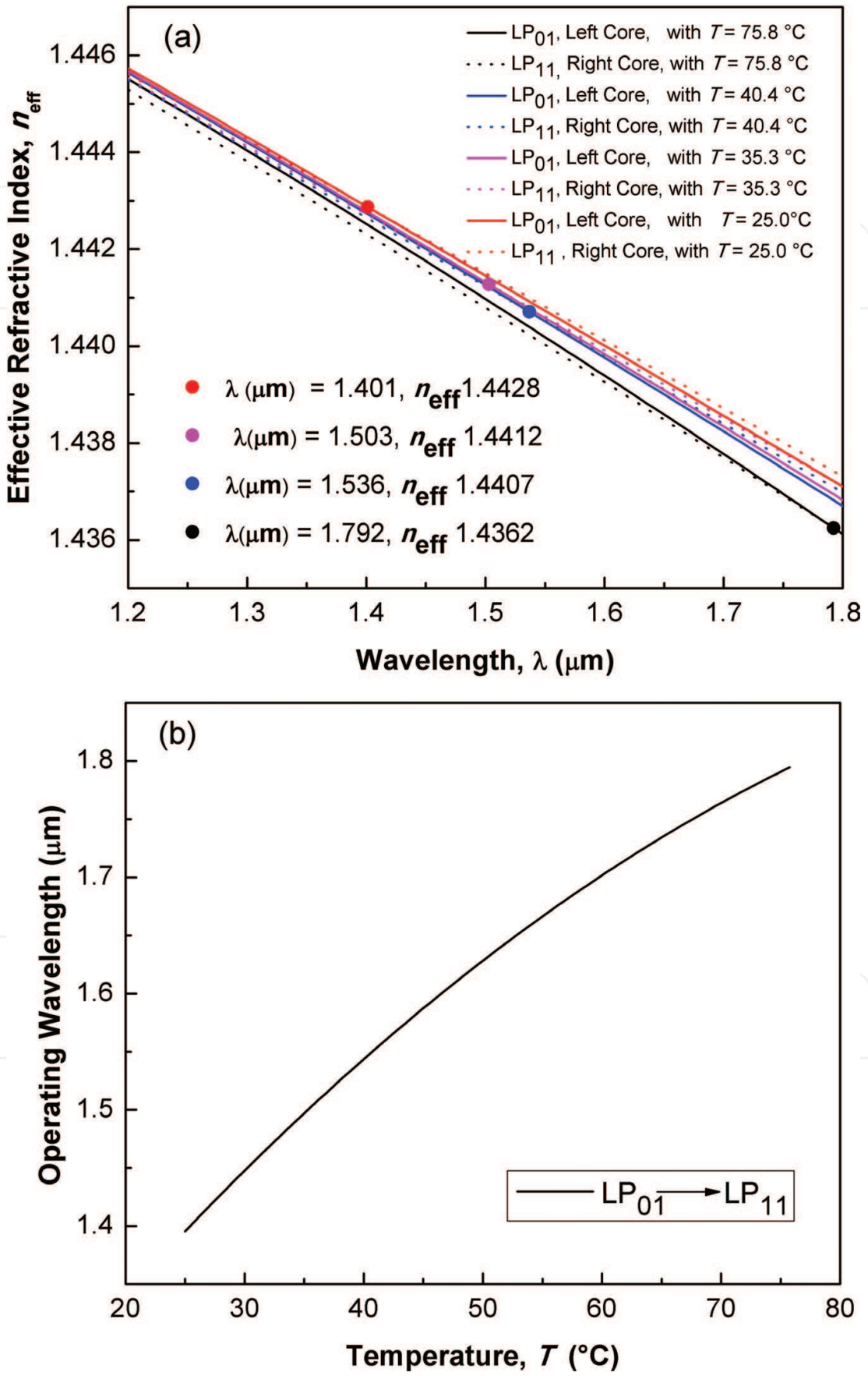

Figure 4. (a) Modal dispersion curves for LP_{01} mode in the left core and LP_{11} in the right core with temperature. (b) Operating wavelength as function of applied temperature on mode converter based on dual-core transversally chirped MOF.

http://dx.doi.org/10.5772/intechopen.70989

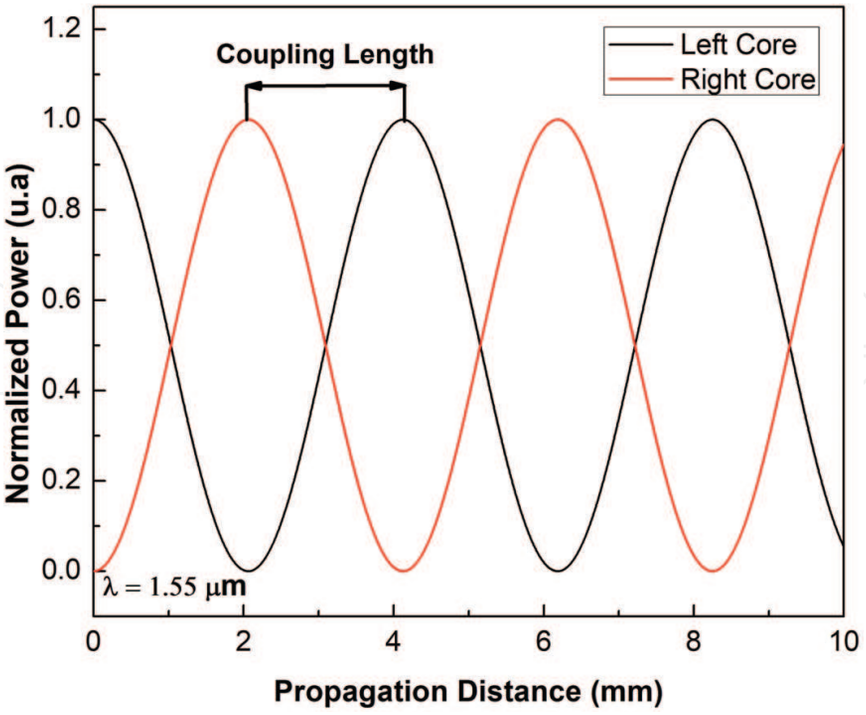

Figure 5. Normalized power transfer for the proposed mode-converter device with $T = 25°C$.

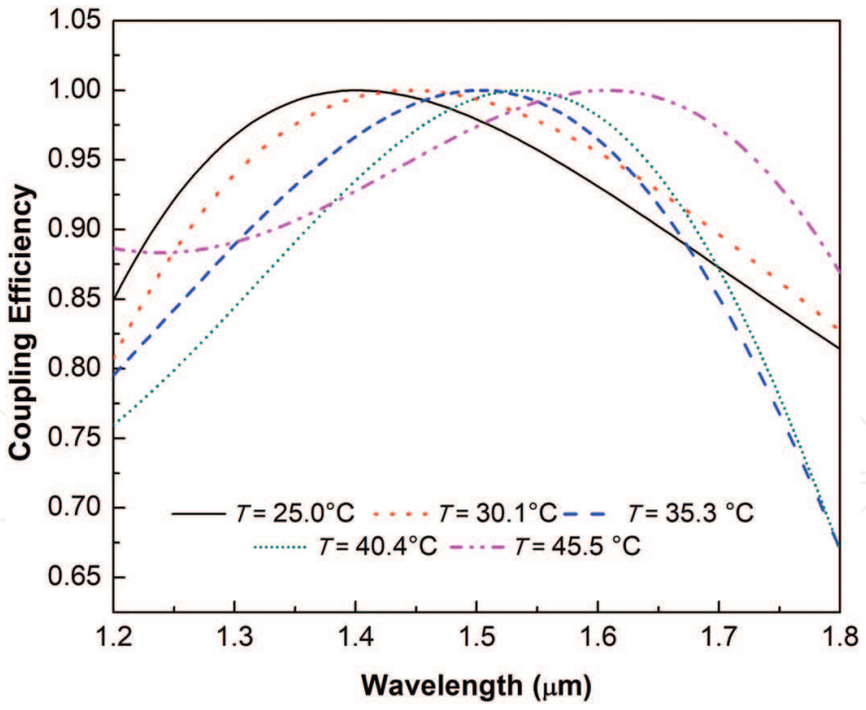

Figure 6. Comparison of mode coupling efficiency for different temperature values in the telecommunication windows.

4. Refractive index sensor

The dual-core transversally chirped MOF that is considered for refractive index sensing of fluids has a similar structure to the fibers in **Figures 1(b)** and **(c)**. Now, it is necessary to guarantee

that the cores are uncoupled to exploit the fiber as a Mach-Zehnder interferometer (MZI) [27]. Then, the distance between the cores is increased to 4Λ, where in this new design Λ = 4.33 μm. This separation was considered because small fluctuations in fiber diameter due to fabrication tolerances may affect the performance of the sensor. In this structure, the diameter of the air holes decreases linearly from d_{max} = 2.6 μm to d_{min} = 0.6 μm, so the relative sizes of holes (d/Λ) range from 0.6 to 0.13 μm. As expected, the cores are non-identical because the holes around the right core are smaller than the holes around the left core. However, both cores are single-mode waveguides due to the slight chirp.

In addition, we consider as an example label-free antibody detection using the highly selective antigen-antibody binding based on our previous experience as another important variation [39]. Then, the first ring of air holes around the right core are functionalized for antibody detection by immobilization of an antigen sensor layer onto the walls of the holes as is shown in **Figure 7**. This layer can consist of a functionalization layer of a certain thickness in addition to the antigen layer. Then, we consider a layer with a thickness t_s equal to 40 nm for sensing the antibody α-streptavidin with thickness t_a = 5 nm. The refractive index of the sensor layer and α-streptavidin is 1.45 (we neglect the dispersion of the biomolecule layer).

From **Figure 8** the operation of the sensor can be clearly understood. The refractometric sensor gains its sensitivity from the fact that only the mode of the right core has substantial overlap with the analyte. This arises because of the low fraction ratio (d/Λ) of holes that surrounding this core. Then the light is not well confined. Now, the RI of the analyte directly modulates the device transmittance by its differential influence on the effective refractive index of each core mode, resulting in a variable phase difference between the optical path lengths of the interferometer arms. Therefore, the proposed configuration was classified as a modal interferometer in the sense that two modes of the dual-core structure are interfering among them. Here, the performance of the sensor is compared with an interesting variation. It consists in

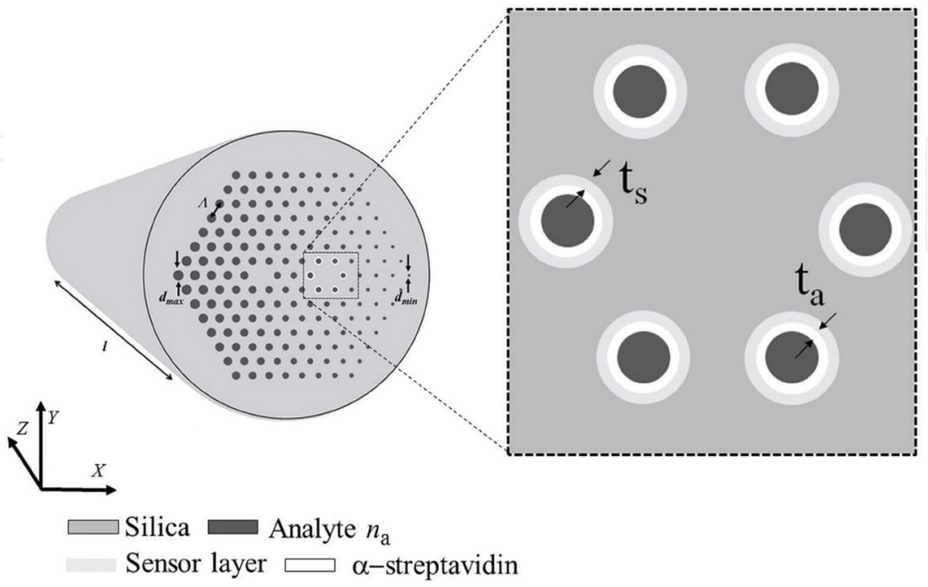

Figure 7. Dual-core transversally chirped MOF biosensor with Λ = 4.33 μm and the hole diameter vary from d_{max} = 2.6 μm to d_{min} = 0.6 μm. In this design, the fiber cores are uncoupled.

http://dx.doi.org/10.5772/intechopen.70989

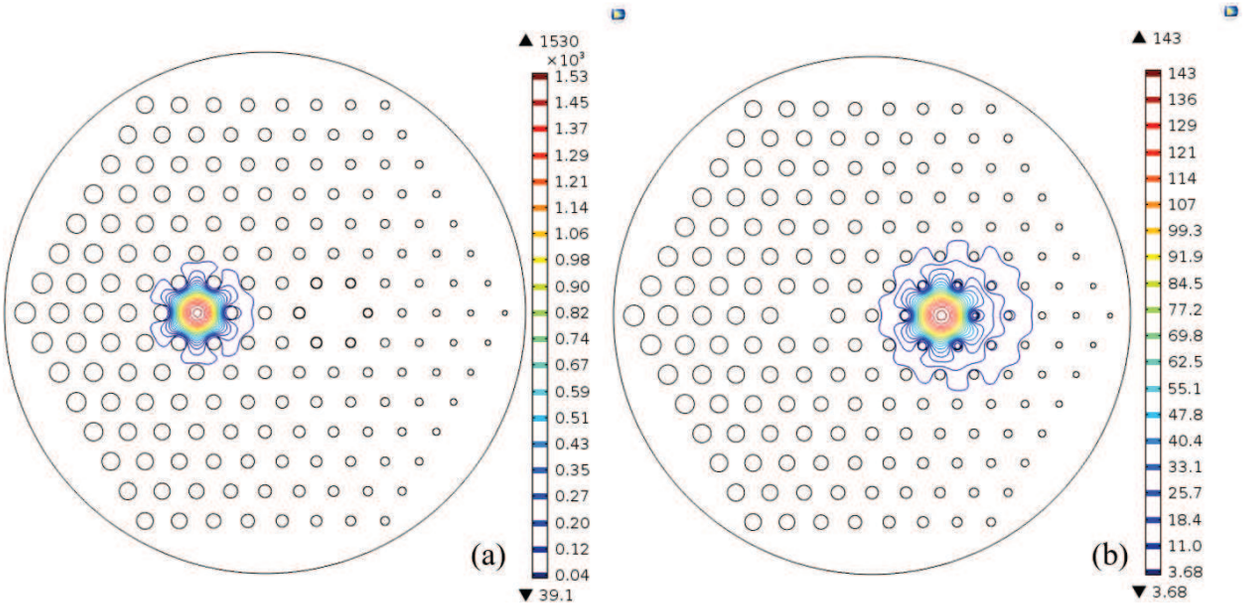

Figure 8. Fundamental mode distribution in left and right core at $\lambda = 633$ nm: Pitch $\Lambda = 4.33$ μm, $d_{max} = 2.6$ μm, $d_{min} = 0.6$ μm; all fiber holes are filled with an analyte of refractive index 1.32.

the inclusion of biomolecule layers onto the walls of the holes, as already explained. We only apply this variation on the first ring of air holes around the right core in order to determine the impact on sensitivity of the proposed sensor.

Figure 9 shows the effective refractive index of each mode when the analyte RI changes from 1.32 to 1.44 at $\lambda = 633$ nm. In this figure, we compared the obtained results of the MZI with and without biomolecule layers onto the walls of the holes. From these results, it is clear that in all cases the effective refractive index increases with the analyte RI. As expected, the behavior of the left core is the same in both configurations, due that this core has good confinement fraction and no biomolecule layer. On the other hand, the results of the right core are different, the results with biomolecule layers presents bigger values in the effective refractive index in the whole range, which indicate that the presence of biomolecules can affect the behavior of our configuration. Although the asymmetric nature of the proposed schematic, the chirped MOF-based interferometer is insensitive to the polarization state of the input beam, as we can see from results illustrated in **Figure 9**. This is a great advantage because our sensor does not require controls of polarization. Then, its implementation could be easier than other configurations.

Figure 10(a) shows the effective refractive index difference between the two fundamental modes—for the two orthogonal polarizations and the two studied configurations—that propagate through the fiber cores as a function of analyte RI. Now, from the effective refractive index difference, it is possible to determine the phase difference per unit length, which is given by Eq. (1). In this equation, Δn_{eff} is the effective refractive index difference between the two fundamental modes that propagate through the fiber cores.

$$\delta = \frac{2\pi \Delta n_{eff}}{\lambda} \tag{1}$$

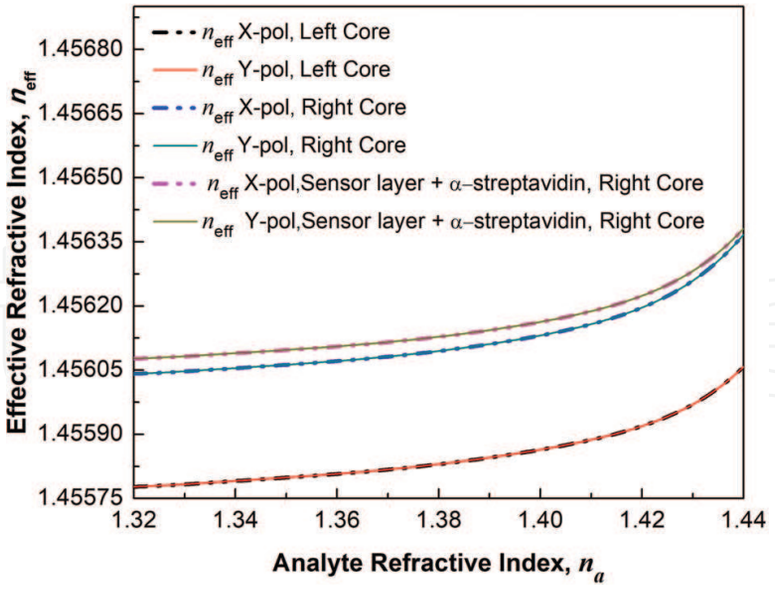

Figure 9. Effective refractive index of the fundamental modes for both polarizations as a function of analyte refractive index. This figure compares obtained results for configurations with and without biomolecules layers.

Figure 10(b) shows the phase difference per unit length as a function of analyte RI. Here, we only present the results for *x*-polarization. As mentioned before, this sensor is polarization-insensitive. As we can see, even though the analyte RI is low, the large differential overlap of the mode cores with the analyte results in a significant amount of phase difference. In both configurations, the phase difference increases exponentially. The configuration with biomolecules layers present higher δ in the whole range compared with the configuration without biomolecule layers. The region from 1.32 to 1.40 presents a phase difference per unit length almost constant in both cases, while for analyte RI higher than 1.40 the phase difference per unit length increases strongly with analyte RI. These results show a better behavior for the

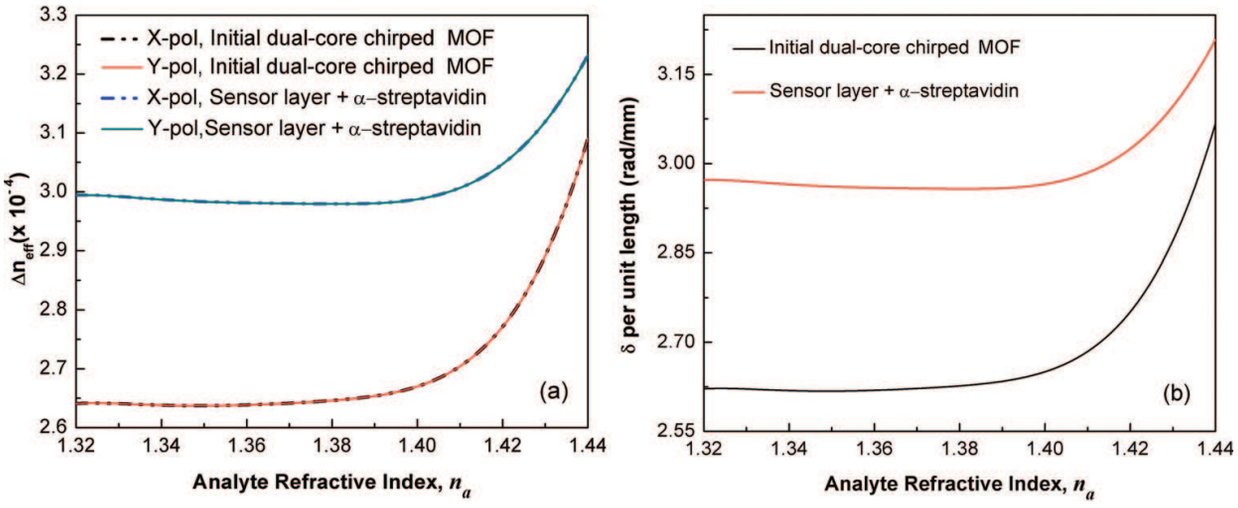

Figure 10. (a) Effective refractive index difference between the two fundamental modes that propagate through the fiber cores as a function of analyte refractive index. (b) Phase difference between the two fundamental modes that propagate through the fiber cores as a function of analyte refractive index (x-polarization).

http://dx.doi.org/10.5772/intechopen.70989

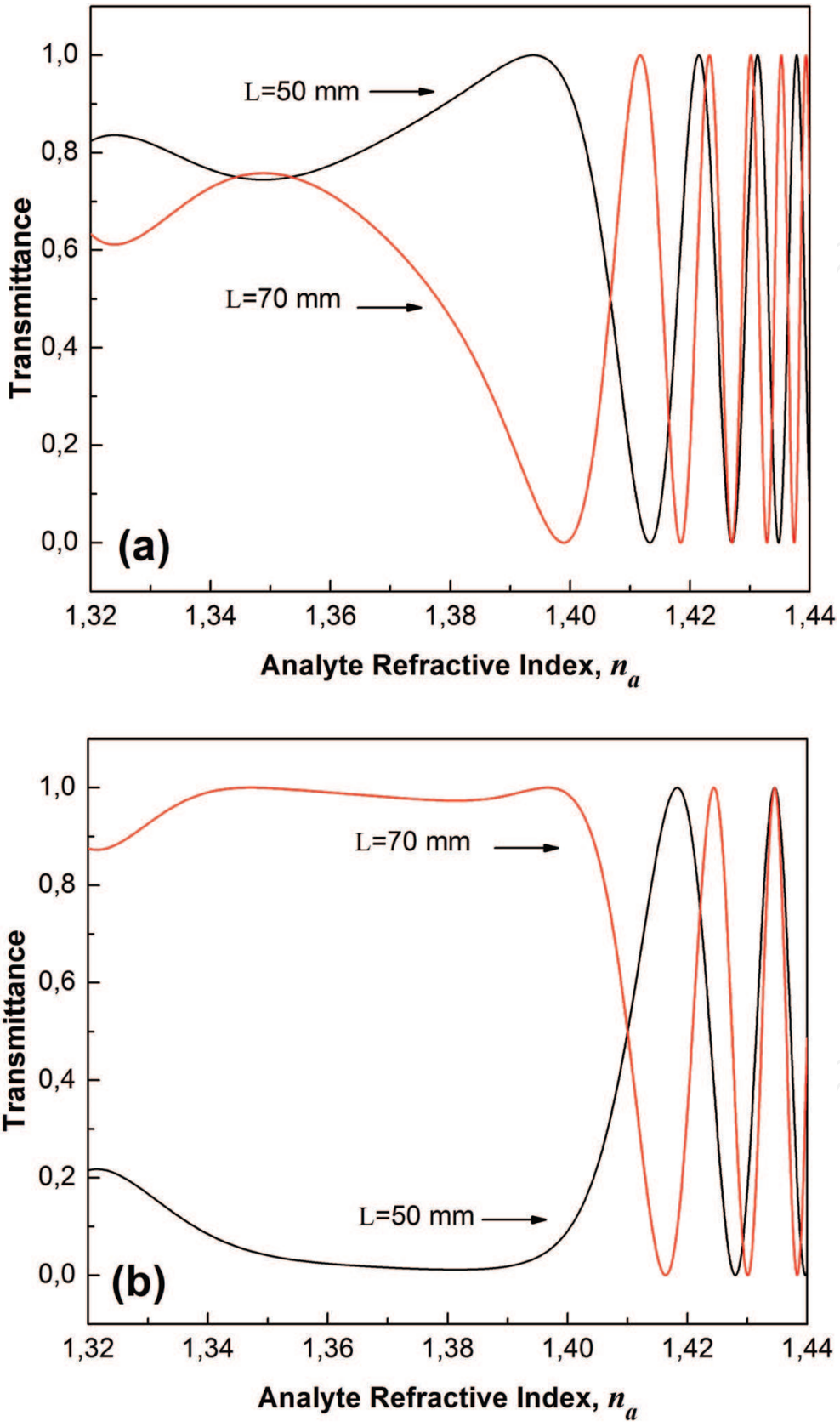

Figure 11. Transmittance of the dual-core transversally chirped MOF for L = 50 mm and L = 70 mm as a function of analyte refractive index: (a) RI sensor without biomolecules layers; (b) RI sensor with biomolecules layers into the first ring of air holes around the right core.

configuration without biomolecules layers. We believe that it is due to that the layers help to confine the light within the right core.

The phase difference per unit length obtained in **Figure 10(b)** was analytically approximated by an exponential function, which was used to obtain the transmittance of the both sensing configurations. For a balanced interferometer, the normalized transmittance can be calculated by using the following expression

$$T = \cos^2\left(\frac{\delta L}{2}\right) \tag{2}$$

where L is the total length of the sensor. Note that as the analyte refractive index increases, the transmittance passes through a series of nulls and peaks as the phase difference increases. In our case, the fact that the periodic variation of transmittance is reducing indicates that the phase difference between the optical paths of the chirped MOF interferometer changes increasingly rapidly with increasing analyte RI. In addition, these results show that the best region to implement the proposed interferometric schemes is for analyte RI from 1.40 to 1.44.

For best sensitivity, the sensor must be biased to operate at 50% transmittance around a given value of refractive index. In practice, this condition may be achieved by fabricating the device with a length so that $\delta = \pi/2$ (plus any multiple of π radians), or by temperature or wavelength tuning. In **Figure 11(a)**, we can see that the sensitivity of the dual-core transversally chirped MOF structure scales with device length. For example, the sensitivity around $n_a = 1.42$ is 3.028×10^2 RIU^{-1} for a 70-mm-long device, which gives a detection limit of 3.303×10^{-6} RIU assuming that we can detect transmittance variations of 10^{-3}. On the other hand, from the **Figure 11(b)** the configuration with biomolecules layers in the first ring of air holes around the right core present a sensitivity equal to 1.83×10^2 RIU^{-1} around $n_a = 1.42$. In this case, the detection limit is 5.464×10^{-6} RIU. Based on the obtained results, it is clear that the best configuration to measure refractive index changes is the scheme without biomolecules layers. In addition, other works presents the same order of sensitivity [44, 59] but using selective filling of some holes of the microstructure in order to improve the sensor performance.

5. Conclusion

In this chapter, we have presented the concept of dual-core transversally chirped microstructured optical fiber and how this structure can be used in different applications such as mode-converter devices and refractive index sensors. We have shown two simple methods to manufacture this specialty fiber. The effect of pressure inside of fiber holes was demonstrated and the transversal chirp of the MOF can be controlled.

Based on this novel concept, a mode selective coupler was designed and analyzed. We demonstrated a promising platform to manufacture compact and highly efficient mode converters. Through the fluid-filling post-processing technique the operating wavelength and the coupling efficiency can be can be continuously tuned by varying the temperature. The coupling efficiency over the entire wavelength range between 1.2 μm and 1.7 μm was greater than 65%.

Consequently, the proposed mode converter can operate in the E + S + C + L + U bands. In general, this kind of mode selective coupler has potential applications in MDM optical fiber communications since it can increase the channel capacity.

Finally, sensing possibilities enabled by the concept of transversally chirped microstructure have been proved, which can be exploited for refractive index sensing in an interferometric arrangement. We have also identified some features of this sensor, including high sensitivity and resolution and scalability of the sensitivity with sensor length. The sensor can be operated over a wide range of analyte refractive index values with a higher sensitivity compared to other selectively filled MOF sensors.

Acknowledgements

This work was supported in part by the Universidad Nacional de Colombia and the Instituto Tecnológico Metropolitano (projects P15108). Erick Reyes-Vera was supported in part by a grant from SPIE.

Author details

Erick Reyes Vera[1,2]*, Juan Úsuga Restrepo[2], Margarita Varon[1] and Pedro Torres[3]

*Address all correspondence to: erickreyes@itm.edu.co

1 Department of Electrical and Electronic Engineering, Universidad Nacional de Colombia, Bogota, Colombia

2 Department of Electronic and Telecommunications, Instituto Tecnológico Metropolitano, Medellín, Colombia

3 Escuela de Física, Universidad Nacional de Colombia, Medellín, Colombia

References

[1] Richardson DJ, Fini JM, Nelson LE. Space-division multiplexing in optical fibres. Nature Photonics. 2013;**7**:354-362

[2] Tkach RW. Scaling optical communications for the next decade and beyond. Bell Labs Technical Journal. 2010;**14**:3-9

[3] Cai S, Yu S, Lan M, Gao L, Nie S, Gu W. Broadband mode converter based on photonic crystal fiber. IEEE Photonics Technology Letters. 2015;**27**:474-477

[4] Schulze C, Bruning R, Schroter S, Duparre M. Mode coupling in few-mode fibers induced by mechanical stress. Journal of Lightwave Technology. 2015;**33**:4488-4496

[5] Zhang Y, Wang Y, Cai S, Lan M, Yu S, Gu W. Mode converter based on dual-core all-solid photonic bandgap fiber. Photonics Research. 2015;**3**:220-223

[6] Yunhe Zhao, Y. Liu, Jianxiang Wen, and Tingyun Wang, Mode converter based on the long period fiber gratings written in two mode fiber, in 2015 Opto-Electronics and Communications Conference (OECC) (IEEE, 2015), Vol. 24, pp. 1-3

[7] Martelli P, Gatto A, Boffi P, Martinelli M. Free-space optical transmission with orbital angular momentum division multiplexing. Electronics Letters. 2011;**47**:972

[8] Weng Y, He X, Wang J, Pan Z. All-optical ultrafast wavelength and mode converter based on inter-modal four-wave mixing in few-mode fibers. Optics Communication. 2015;**348**:7-12

[9] Hellwig T, Walbaum T, Fallnich C. Optically induced mode conversion in graded-index fibers using ultra-short laser pulses. Applied Physics B: Lasers and Optics. 2013;**112**:499-505

[10] Shi CX, Okoshi T. Mode conversion based on the periodic coupling by a reflective fiber grating. Optics Letters. 1992;**17**:1655-1657

[11] Usuga J, Amariles D, Correa N, Reyes-Vera E, Gomez-Cardona N. Analysis of chromatic dispersion compensator using a PCF with elliptical holes. Revista Colombiana de Física. 2016;**33**:38-41

[12] Birks TA, Knight JC, Russell PSJ. Endlessly single-mode photonic crystal fiber. Optics Letters. 1997;**22**:961

[13] Ortigosa-Blanch A, Knight JC, Wadsworth WJ, Arriaga J, Mangan BJ, Birks TA, Russell PS. Highly birefringent photonic crystal fibers. Optics Letters. 2000;**25**:1325-1327

[14] Eggleton B, Kerbage C, Westbrook P, Windeler R, Hale A. Microstructured optical fiber devices. Optics Express. 2001;**9**:698

[15] Reyes-Vera E, Gonzalez-Valencia E, Torres P. Understanding the birefringence effects in an all-fiber device based on photonic crystal fibers with integrated electrodes. Photonics Letters of Poland. 2010;**2**:168-170

[16] Reyes-Vera E, Gonzalez-Valencia E, Torres P. Transverse stress response of FBGs in large-mode-area microstructured Panda-type fibers. In: Hernández-Cordero J, Torres-Gómez I, Méndez A, editors. Proceedings of SPIE. Vol. 7839. 2010. p. 78391G

[17] Reyes-Vera E, Torres P. Influence of filler metal on birefringent optical properties of photonic crystal fiber with integrated electrodes. Journal of Optics. 2016;**18**:85804

[18] Khaleque A., Franco MAR, and Hattori H, Ultra-broadband and compact polarization splitter for sensing applications, in Photonics and Fiber Technology 2016 (ACOFT, BGPP, NP) (OSA, 2016), Vol. 2, p. JM6A.2

[19] Franco MAR, Serrão VA, Sircilli F. Microstructured optical fiber for residual dispersion compensation over S+C+L+U Wavelength Bands. IEEE Photonics Technology Letters. 2008;**20**:751-753

[20] Betancur-Pérez AF, Botero-Cadavid JF, Reyes-Vera E, Gómez-Cardona N. Hexagonal photonic crystal fiber behaviour as a chromatic dispersion compensator of a 40 Gbps link. International Journal of Electronics and Telecommunications. 2017;**63**:93-98

[21] Chen MY, Chiang KS. Mode-selective characteristics of an optical fiber with a high-index core and a photonic bandgap cladding. IEEE Journal of Selected Topics in Quantum Electronics. 2016;**22**:251-257

[22] Huang W, Liu Y, Wang Z, Zhang W, Luo M, Liu X, Guo J, Liu B, Lin L. Generation and excitation of different orbital angular momentum states in a tunable microstructure optical fiber. Optics Express. 2015;**23**:33741-33752

[23] Cai S, Yu S, Wang Y, Lan M, Gao L, Gu W. Hybrid dual-core photonic crystal fiber for spatial mode conversion. IEEE Photonics Technology Letters. 2016;**28**:339-342

[24] Reyes Vera EE, Usuga Restrepo JE, Gómez Cardona NE, and Varón M. Mode selective coupler based in a dual-core photonic crystal fiber with non-identical cores for spatial mode conversion, in Latin America Optics and Photonics Conference (OSA, 2016), p. LTu3C.1

[25] Frazão O, Santos JL, Araújo FM, Ferreira LA. Optical sensing with photonic crystal fibers. Laser & Photonics Reviews. 2008;**2**:449-459

[26] Torres P, Reyes-Vera E, Díez A, Andrés MV. Two-core transversally chirped microstructured optical fiber refractive index sensor. Optics Letters. 2014;**39**:1593-1596

[27] Rindorf L, Bang O. Sensitivity of photonic crystal fiber grating sensors: biosensing, refractive index, strain, and temperature sensing. Journal of the Optical Society of America B: Optical Physics. 2008;**25**:310

[28] Zhang X, Peng W. Fiber Bragg grating inscribed in dual-core photonic crystal fiber. IEEE Photonics Technology Letters. 2015;**27**:391-394

[29] Reyes-Vera E, Cordeiro CMB, Torres P. Highly sensitive temperature sensor using a Sagnac loop interferometer based on a side-hole photonic crystal fiber filled with metal. Applied Optics. 2017;**56**:156

[30] Villatoro J, Minkovich VP, Zubia J. Photonic crystal fiber interferometric force sensor. IEEE Photonics Technology Letters. 2015;**27**:1181-1184

[31] Villatoro J, Minkovich VP, Zubia J. Photonic crystal fiber interferometric vector bending sensor. Optics Letters. 2015;**40**:3113

[32] Osório JH, Hayashi JG, Espinel YAV, Franco MAR, Andrés MV, Cordeiro CMB. Photonic-crystal fiber-based pressure sensor for dual environment monitoring. Applied Optics. 2014;**53**(3668)

[33] Wang J-N, Tang J-L. Photonic crystal fiber Mach-Zehnder interferometer for refractive index sensing. Sensors (Basel). 2012;**12**:2983-2995

[34] Silva S, Roriz P, Frazão O. Refractive index measurement of liquids based on microstructured optical fibers. Photonics. 2014;**1**:516-529

[35] Oliveira R, Osório JH, Aristilde S, Bilro L, Nogueira RN, Cordeiro CMB. Simultaneous measurement of strain, temperature and refractive index based on multimode interference, fiber tapering and fiber Bragg gratings. Measurement Science and Technology. 2016;**27**:75107

[36] Osório JH, Oliveira R, Aristilde S, Chesini G, Franco MAR, Nogueira RN, Cordeiro CMB. Bragg gratings in surface-core fibers: Refractive index and directional curvature sensing. Optical Fiber Technology. 2017;**34**:86-90

[37] Markos C, Yuan W, Vlachos K, Town GE, Bang O. Label-free biosensing with high sensitivity in dual-core microstructured polymer optical fibers. Optics Express. 2011; **19**(7790-8)

[38] Reyes-Vera E, Gómez-Cardona N, Torres P. Label-free biosensor based on a dual-core transversally chirped microstructured optical fiber. In: López-Higuera JM, Jones JDC, López-Amo M, Santos JL, editors. Proceedings of SPIE. Vol. 9157. 2014 91578J

[39] Monro TM, Belardi W, Furusawa K, Baggett JC, Broderick NGR, Richardson DJ. Sensing with microstructured optical fibres. Measurement Science and Technology. 2001;**12**: 854-858

[40] Mägi E, Steinvurzel P, Eggleton B. Tapered photonic crystal fibers. Optics Express. 2004; **12**(776-84)

[41] Velasquez-Botero F, Reyes-Vera E, Torres P. Some refractometric features of dual-core chirped microstructured optical fibers. In: Kalinowski HJ, Fabris JL, Bock WJ, editors. Proceedings of SPIE. Vol. 9634. 2015 963450

[42] Wu DKC, Kuhlmey BT, Eggleton BJ. Ultrasensitive photonic crystal fiber refractive index sensor. Optics Letters. 2009;**34**:322

[43] Kuhlmey BT, Coen S, Mahmoodian S. Coated photonic bandgap fibres for low-index sensing applications: cutoff analysis. Optics Express. 2009;**17**:16306-16321

[44] Sun B, Chen M-Y, Zhang Y-K, Yang J-C, Yao J, Cui H-X. Microstructured-core photonic-crystal fiber for ultra-sensitive refractive index sensing. Optics Express. 2011; **19**(4091-4100)

[45] Matuschek N, Kartner FX, Keller U. Analytical design of double-chirped mirrors with custom-tailored dispersion characteristics. IEEE Journal of Quantum Electronics. 1999;**35**:129-137

[46] Riant I, Gurib S, Gourhant J, Sansonetti P, Bungarzeanu C, Kashyap R. Chirped fiber Bragg gratings for WDM chromatic dispersion compensation in multispan 10-Gb/s transmission. IEEE Journal of Selected Topics in Quantum Electronics. 1999;**5**:1312-1324

[47] Skibina JS, Iliew R, Bethge J, Bock M, Fischer D, Beloglasov VI, Wedell R, Steinmeyer G. A chirped photonic-crystal fibre. Nature Photonics. 2008;**2**:679-683

[48] Ghosh S, Varshney RK, Pal BP, Monnom G. A Bragg-like chirped clad all-solid microstructured optical fiber with ultra-wide bandwidth for short pulse delivery and pulse reshaping. Optical and Quantum Electronics. 2010;**42**:1-14

[49] Russell PSJ. Photonic-crystal fibers. Journal of Lightwave Technology. 2006;**24**:4729-4749

[50] Méndez A, Morse TF. Specialty Optical Fibers Handbook. London, Academic Press; 2007

[51] Bansal NP. Handbook of Glass Properties. London, Academic Press; 1986

[52] Du F, Lu Y-Q, Wu S-T. Electrically tunable liquid-crystal photonic crystal fiber. Applied Physics Letters. 2004;**85**:2181-2183

[53] Larsen T, Bjarklev A, Hermann D, Broeng J. Optical devices based on liquid crystal photonic bandgap fibres. Optics Express. 2003;**11**(2589-96)

[54] Alkeskjold TT, Lægsgaard J, Bjarklev A, Hermann DS, Anawati A, Broeng J, Li J, Wu S-T. All-optical modulation in dye-doped nematic liquid crystal photonic bandgap fibers. Optics Express. 2004;**12**:5857

[55] Steinvurzel P, Eggleton BJ, de Sterke CM, Steel MJ. Continuously tunable bandpass filtering using high-index inclusion microstructured optical fibre. Electronics Letters 2005;**41**:463

[56] Alkeskjold TT, Bjarklev A. Electrically controlled broadband liquid crystal photonic bandgap fiber polarimeter. Optics Letters. 2007;**32**:1707

[57] Snyder AW, Love JD. Optical Waveguide Theory. New York, Springer US; 1983

[58] Lee DL. Electromagnetic Principles of Integrated Optics. 1st ed. New Jersey, Wiley; 1986

[59] Wu Y, Town GE, Bang O. Refractive index sensing in an all-solid twin-core photonic bandgap fiber. IEEE Sensors Journal. 2010;**10**:1192-1199

IntechOpen